A Numerical Study of Buried Biomass Effects on Ground-Penetrating Radar Performance

Nakasit Niltawach, Chi-Chih Chen, *Member, IEEE*, Joel T. Johnson, *Senior Member, IEEE*, and Brian A. Baertlein, *Member, IEEE*

***Abstract*—It is widely acknowledged that tree roots and other forms of buried biomass can have an adverse effect on the performance of ground-penetrating radars (GPRs). In this paper, we present analyses that examine that effect for ground-contacting GPR systems. A test site containing extensive root infiltration at Eglin Air Force Base, FL, was excavated, and the root structure and soil were thoroughly characterized. A numerical simulator based on the discrete dipole approximation, which is an integral-equation-based method, was developed, validated, and subsequently used to compute scattering from root structures modeled by an ensemble of buried cylinders. An examination of the results is presented that quantifies the potential for false alarms and increased clutter due to buried roots.**

***Index Terms*—Biomass, discrete dipole approximation (DDA), ground-penetrating radar (GPR), roots, unexploded ordnance (UXO).**

I. Introduction

GROUND-penetrating radar (GPR) is widely used for detecting and monitoring subsurface objects. There is extensive anecdotal evidence that biomass (i.e., plant and tree roots) adversely affects GPR performance. Biomass has been implicated in both false alarms and impaired detection performance, but, surprisingly, there has been scant research into this topic. In this paper, we present a numerical model for root scattering that is capable of handling arbitrarily complicated root structures. The results of the simulator are validated by comparison with experimental results from a specific GPR and are applied in a study of root clutter from a specific site.

Scattering from roots is highly dependent on frequency and on the root permittivity with respect to that of the background soil. Because microwave attenuation in soil rapidly increases with frequency, essentially all GPRs capable of interacting with roots operate at frequencies below approximately 5 GHz. The frequency range used in our study is below 2 GHz. In this regime, the roots tend to be electrically thin, and this fact is used at several points in this analysis.

Scattering from buried objects in general has been studied extensively, because of its many applications including archaeology, law enforcement, remote sensing, and geological exploration [1]–[10]. The targets of interest include both dielectric and conducting objects. Buried-target numerical scattering models often involve Sommerfeld-like integrals, which are time-consuming to evaluate, and fast algorithms have been developed for those integrals [11], [12]. In general, previous works are restricted to a single object and limited ranges of permittivities and object sizes. Although many studies of scattering from dielectric objects under a half-space have appeared, few of these specifically address tree roots. Sullivan [13] modeled tree roots as an ensemble of connected cylinders without including interaction between each root. El-Shenawee *et al.* [14] modeled a dielectric clutter object (which could be a tree root) close to an antipersonnel mine-like object under a rough surface. However, neither of these references utilized realistic root geometries in their studies.

This paper is organized as follows. In Section II, we review an experiment in which a high biomass density site was excavated to obtain information on buried biomass properties; a small set of ground-contacting GPR data from this site is also described. The nature of the antenna of interest permits a simplification of the problem that we exploit in our solution procedure. In Section III, the scattering behavior of a realistic cluster of roots is investigated numerically using the discrete dipole approximation (DDA) [15], [16]. Results for scattering from finite, circular, dielectric cylinders calculated using DDA show excellent agreement with measurements in a laboratory validation, and in comparisons with results calculated via alternate method of moments codes. In Section IV, scattering from a realistic root structure is computed to study its impact on the detection of a buried 105-mm unexploded ordinance (UXO). Concluding remarks appear in Section V.

II. Experimental Work

During previous GPR experiments performed by the U.S. Army Research Laboratory (ARL) at Eglin AFB, impaired performance was noted at a particular site. A subsequent excavation of the site revealed a high density of roots. A team from Ohio State University (OSU) returned to Eglin AFB for additional tests. Soil was removed from a site of area 2 m $\times$ 2 m; the excavated area containing a high density of roots is shown in Fig. 1. Most of the roots were found near a depth of 15 cm. Essentially no roots were found below a depth of 30 cm.

Roots from the site were removed, bagged, and later analyzed for their moisture content and size distribution. Dielectric properties of the soil at the site were also analyzed [17], [18]

Although not described in detail here, a small set of GPR measurements were performed at this site with the ground-contacting antenna shown in Fig. 2. Measurements occurred prior to excavation of the site, so that information on the distribution

Manuscript received July 2, 2003; revised January 15, 2004. This work was supported by the U.S. Army Research Office under Contract DAAD19-01-1-0760 and Project E-43042-EL-000-01234-1 with support from the U.S. Army Research Laboratory, Radar Branch.

The authors are with the ElectroScience Laboratory, The Ohio State University, Columbus, OH 43212 USA.

Digital Object Identifier 10.1109/TGRS.2004.825582

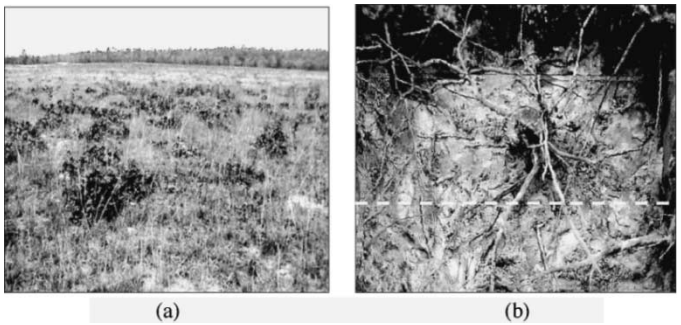

Fig. 1. Measurement site (a) before and (b) after removing the topsoil. In (b), the area imaged is approximately 2×2 m^2. The dashed line illustrated is the scan path for GPR measurements.

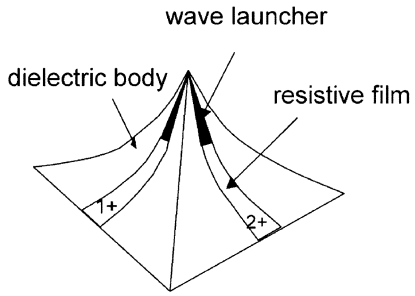

Fig. 2. Broadband dual-polarized dielectric horn antenna used in our studies.

of subsurface biomass was not available. Unfortunately, the resulting data were obtained from a scan over locations in Fig. 1(b) with only low biomass densities, so that significant information on biomass effects was not obtained from the dataset. The "ground truth" root physical data obtained in the experiment, however, still allowed a modeling analysis of these effects to proceed, assuming that the model's predictions could be verified versus GPR measurements through an alternate process. The antenna used is a broadband, dual-polarization, dielectric-loaded horn antenna developed at the OSU ElectroScience Laboratory (ESL) [19]. The antenna loading was selected to match that of the soil (dielectric constant 5), with the result that reflections from the ground surface are minimized.[1] This nature of the antenna has implications for modeling. Because the antenna minimizes reflections at the soil surface, the measured data approximate those that would be collected by an antenna immersed in unbounded soil (i.e., without the air-soil interface). In the analysis that follows, that simplification is used extensively.

III. DDA Formulation of Root Scattering

A simple analysis of scattering from thin dielectric cylindrical structures can provide some information about expected properties of root effects [20]–[23, Sec. 4.1.3.2], if it is assumed that the transmitting antenna is sufficiently far from the root to approximate a planar incident field. Scattered fields in this limit depend quadratically on the effective root radius relative to the observing wavelength in the background medium. The effective root radius is the true root radius multiplied by a function of the ratio of the root to background medium dielectric constants, with a differing function for parallel (electric field along the root length) and perpendicular polarizations. For wet roots with large dielectric constants relative to the background medium, the parallel polarized component is dominant. Alternately, for ratios of root to background medium dielectric constants less than one, scattering is larger for the perpendicular polarization. It can also be shown that root radius does not have a significant effect on the polarization ratio in the small-root approximation. Although this simple analysis provides some insight into the fundamental scattering behavior of an isolated root, it is incapable of describing the effects of realistic root structures.

[1]Because of imperfect matching and irregularities in the surface topography, a small residual reflection is always present. If wideband waveforms are used and the targets of interest are not too close to the surface, that reflection is easily gated out of the measurements.

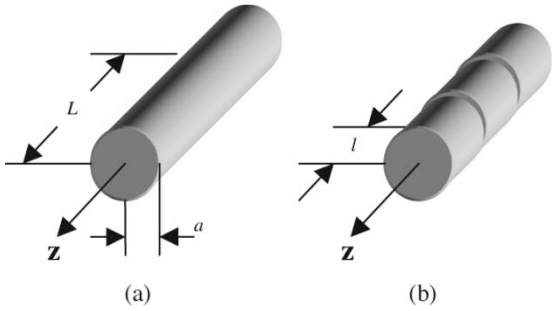

Fig. 3. (a) Thin cylinder with radius a and length L. (b) Segmentation of the cylinder into small cells of length l.

In this section, we present a numerical method for predicting scattering from arbitrary root structures. Because root structures can be very extensive, an efficient method is required. An integral equation approach known as the discrete dipole approximation [16] is employed in this work. It is an efficient method for computing fields scattered from complicated dielectric bodies, and it addresses interactions among all parts of the bodies. In this section, we present the DDA formulation, discuss its efficiency, and validate its performance using measured data and independent calculations.

A. Formulation

The derivation of the DDA begins with the standard electric-field volume integral equation, given by

$$\overline{E}(\overline{r}) = \overline{E}^{\text{inc}} + \int_V dv' \overline{\overline{G}}(\overline{r}, \overline{r}') \cdot k^2 \left(\varepsilon_c(\overline{r}') - 1\right) \overline{E}(\overline{r}') \quad (1)$$

where

$$\overline{\overline{G}}(\overline{r}, \overline{r}') = \left(\overline{\overline{I}} + \frac{\nabla\nabla}{k^2}\right) \frac{e^{-ik|\overline{r}-\overline{r}'|}}{|\overline{r}-\overline{r}'|} \quad (2)$$

is the dyadic Green's function, $\overline{E}^{\text{inc}}$ is the incident electric field, k is the wavenumber in the background medium (dielectric constant ε_m), and the ratio of the root dielectric constant to that of the background medium is denoted as $\varepsilon_c(\overline{r})$. Equation (1) will now be discretized and evaluated numerically using the DDA algorithm. The induced polarization density $\overline{P}$ can be expressed as a function of $\overline{E}$ as

$$\frac{\overline{P}(\overline{r})}{\varepsilon_m} = \left(\varepsilon_c(\overline{r}) - 1\right) \overline{E}(\overline{r}). \quad (3)$$

The volume V is discretized into volumes ΔV_j with centers at $\overline{r}_j$, $j = 1, 2, \ldots, N$, where N is the number of dipoles. The

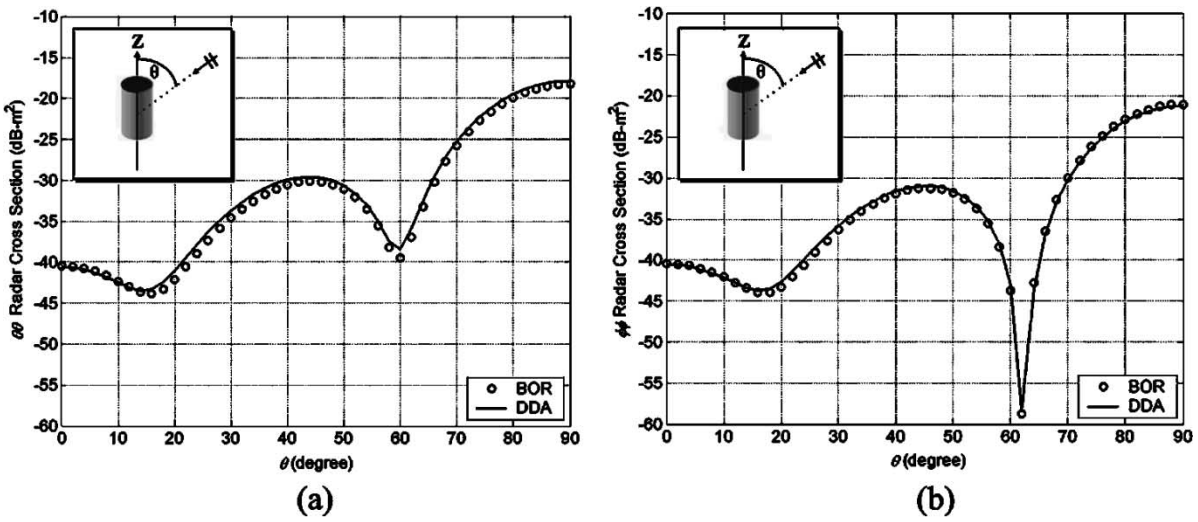

Fig. 4. Comparisons of RCSs computed by DDA and BOR at frequency 1 GHz for a 0.3–m-long 3.96-cm-radius cylinder with relative permittivity 2 (seven-component cylinder). (a) $\theta\theta$ polarization. (b) $\phi\phi$ polarization.

dipole moment inside ΔV_j is further approximated as a constant $\overline{p}_j$ ("pulse expansion"), producing a system of equations

$$\sum_{j=1}^{N} \overline{\overline{A}}(\overline{r}_i, \overline{r}_j) \cdot \overline{p}_j = \overline{E}^{inc}(\overline{r}_i). \tag{4}$$

From (4), it is evident that the scattering problem reduces to finding the polarizations $\overline{p}_j$ that satisfy a system of $3N$ complex linear equations $[\overline{\overline{A}}] \cdot [\overline{p}] = [\overline{E}^{\text{inc}}]$. Once $\overline{p}_j$ is found, one can approximate the scattered fields by

$$\overline{E}_s(\overline{r}) \approx \sum_{j=1}^{N} \overline{\overline{A}}(\overline{r}, \overline{r}_j) \cdot \overline{p}_j. \tag{5}$$

The matrix elements are evaluated as follows. First, consider a thin cylinder with radius a and length $L \gg a$ as shown in Fig. 3(a). If the cylinder is also electrically thin with $ka \ll 1$, the current over each cross section is approximately uniform, and only the longitudinal variation in $\overline{p}$ is of interest. Cylinders are segmented as shown in Fig. 3(b) to ensure each segment length is also much smaller than a wavelength. For $\overline{r}_i \neq \overline{r}_j$, the above formulation assumes that the matrix elements are given by

$$\overline{\overline{A}}_{ij} = \frac{-k^2}{\varepsilon_m} \int\limits_{\Delta v_j} dv' \overline{\overline{G}}(r_i, \overline{r}') \approx \frac{-k^2}{\varepsilon_m} \overline{\overline{G}}(\overline{r}_i, \overline{r}_j) \Delta V_j = \overline{\overline{A}}(\overline{r}_i, \overline{r}_j). \tag{6}$$

This approximation is not accurate if $\overline{r}_i$ and $\overline{r}_j$ are within some small distance r_d [24]. One can improve the accuracy by applying numerical integration over the volume V_j centered at $\overline{r}_j$. An improved evaluation of the matrix terms is then given by

$$\overline{\overline{A}}_{ij} = \begin{cases} \frac{1}{\Delta V_j} \int\limits_{v_j} dv' \overline{\overline{A}}(\overline{r}_i, \overline{r}') & \text{for } |\overline{r}_i - \overline{r}_j| < r_d \\ \overline{\overline{A}}(\overline{r}_i, \overline{r}_j) & \text{for } |\overline{r}_i - \overline{r}_j| \geq r_d. \end{cases} \tag{7}$$

For a thin cylinder, a suitable limit is $r_d = \lambda_m/8$ where λ_m is the wavelength in the background medium. For $\overline{r}_i = \overline{r}_j$ (the "self-term"), an appropriate exclusion volume must be defined. Since scattering from cylinders is of interest here, it is natural to take the exclusion volume to be a circular cylinder. Expressions for the "self-term" in this case are provided in [17] and [18].

The thin-cylinder criterion assumed in DDA requires that the length and diameter of each cell must be small compared to the wavelength of the incident field. Thus, we require $\sqrt{\varepsilon_C} k(2a_{\max}) \leq 1$ and $\sqrt{\varepsilon_C} k l_{\max} \leq 1$. For a cylinder with radius $a > a_{\max}$, we approximate the larger cylinder by an ensemble of densely packed thinner cylinders of the same length such that the volumes of the two configurations are approximately equal. Results illustrating that this approach is reasonable are provided in the next section.

Fig. 1(b) suggests that many cylinders (i.e., large N) will be necessary to represent a realistic root structure. Storage of the resulting matrix is a concern. For N dipoles, the complex matrix $[\overline{\overline{A}}]$ requires $3N \times 3N \times 8$ bytes for four-byte floating-point values. As an example, 2000 dipoles require 288 MB of memory. To reduce the memory usage, only those terms $\overline{\overline{A}}_{ij}$ that require numerical integration are stored. Terms that can be expressed in closed form are recalculated every time they are used.

The system of complex linear equations in (4) must be solved to find the polarization $\overline{p}_j$. An iterative solver is used here instead of a direct method, because iteration is more efficient when the number of dipoles is large. The biconjugate gradient stabilized method was chosen here, since it has been shown to converge more rapidly for DDA than other methods [25]. The iterative solver terminates when $\|[\overline{\overline{A}}] \cdot [\overline{p}] - [\overline{E}^{\text{inc}}]\| \leq e\|\overline{E}^{\text{inc}}\|$ is satisfied, where e is an error criterion, chosen to be 10^{-3} in this work.

B. Comparison With Independent Calculations

The DDA code was compared with the Boeing "Body of Revolution (BOR)" code for cylinders of different radii. That BOR code is based on research by Putnam *et al.* [26], Andreasen [27], and Mautz *et al.* [28]. As a test of DDA, a cylinder of radius 3.96 cm was represented by seven hexagonally packed cylinders of radius 1.5 cm. The result in Fig. 4 shows good agreement for copolarized ($\theta\theta$ and $\phi\phi$) backscattered radar cross sections (RCSs) calculated from the DDA and BOR codes for a segment

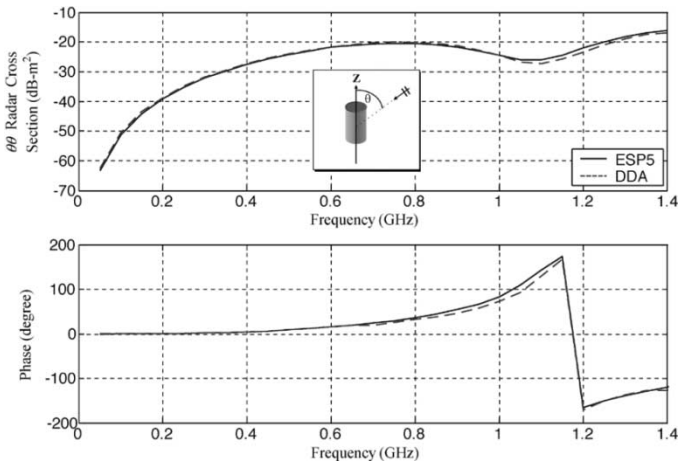

Fig. 5. $\theta\theta$-component(top) amplitude and (bottom) phase of the RCS for a short dielectric cylinder computed by DDA and MOM (OSU/ESP). $\theta = 90°$, length $= 0.2$ m, radius 6.67 cm, and $\varepsilon_c = 2$.

length of 0.3 m at 1 GHz. Fig. 4 indicates that thick cylinders can be reasonably approximated by an ensemble of thinner cylinders. For this case, the number of unknowns is 63.

The efficiency of the DDA code was explored via a comparison with a conventional MoM code. We computed the copolarized $(\theta\theta)$ RCS for normal incidence on a short cylinder with length 0.2 m and radius 6.67 cm. The calculation was performed from 0.05–1.40 GHz using both the DDA code and OSU's Electromagnetic Surface Patch (ESP) code [29]. Fig. 5 shows good agreement in the two computed results. The computation times were 17 min and 7.9 h, for the DDA and ESP codes, respectively, on a 1.60-GHz Pentium 4 computer with 256 MB memory. This is not an entirely fair comparison, because DDA uses an iterative method to solve its linear equations, while ESP employs LU decomposition of its impedance matrix. Nonetheless, the dramatic difference in computation time suggests that DDA is a good candidate for root structures and other large problems.

C. Validation for Modeling GPR Measurements

Unlike the field data collection described in Section II, GPR validation measurements were performed in a controlled environment comprised of homogeneous, dry sand with a smooth level surface (see Fig. 6). In the DDA simulation, the antenna was represented by two orthogonal dipole elements oriented parallel and perpendicular to the direction of the scan. The true pattern of the GPR antenna is somewhat different from that of a dipole, but it will be shown later that this simplification is reasonably accurate. A complete model of this antenna on an air–ground interface has been obtained using a three-dimensional finite-difference time domain (FDTD) approach [30], but the dipole approximation is sufficiently accurate and vastly more efficient for our purposes.

Backscatter measurements for several long dielectric cylinders were collected. The cylinders had diameters of 1.2 cm (0.5 in) and 2.5 cm (1 in), with dielectric constants of 2.2 (a solid acrylic cylinder) and 30 (a methanol-filled tube). The cylinders were individually inserted horizontally into the soil from the side of the test site to avoid any digging-related soil disturbance. Before inserting the cylinders, a background

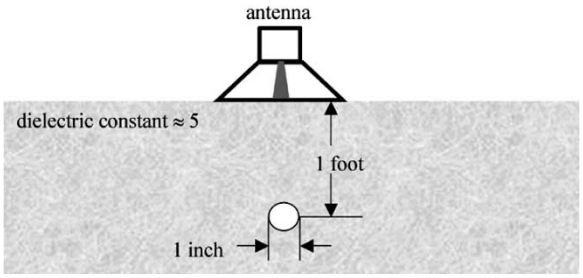

Fig. 6. Equipment configuration for dielectric cylinder measurements.

measurement was collected and later subtracted from the data. The antenna remained stationary during these measurements with one dipole axis collinear with the cylinder. An additional calibration measurement was performed using a long thin conducting wire laid on the ground surface under the antenna. The wire was kept straight and oriented in the middle of the two antenna polarizations. Using the known response of a long wire, one can calibrate out the antenna frequency response [31]. The resulting data are referred to as a "scaled backscattered field" because an absolute calibration was not available in the measurement.

Fig. 7 compares the measured and calculated results for rods with dielectric constant of 30, but different diameters, 0.5 and 1 in. Fig. 8 shows a similar comparison for two rods with the same diameter (1 in), but different dielectric constants (2.2 and 30). In these results, the calculated data have been weighted by a frequency-independent "calibration factor" for comparison with measured scaled field values; the same calibration factor is used in all the cases illustrated. The measured data are seen to agree very well with the DDA results, both in the frequency and time domains. The larger errors observed at lower frequencies are influenced by time gating of the measured data required to remove contributions from the antenna mismatch. This time gating results in a convolution of frequency domain data with a window having a 3-dB bandwidth of 0.65 GHz, which distorts the final frequency response in regions with higher rates of change versus frequency. Overall, the level of agreement observed clearly verifies the ability of the model to produce reasonable predictions of ground-contacting GPR measurements.

IV. Biomass Effect on UXO Detectability

Having verified the DDA code, we now use that code to study the effects of root-related clutter and propagation loss for realistic high-density root structures. The objective of this paper is an understanding of the reduction in detection performance caused by root-related clutter and propagation losses. Obtaining reliable estimates of these effects requires a statistically meaningful sample of root configurations. Excavation and mensuration of intact dense root structures is a costly, laborious, time-consuming operation. For the study described here, the only sample available to us is that shown in Fig. 1(b), and all of our results are based solely on that sample. For that reason, the results presented here should be viewed as suggestive rather than definitive.

The structure of Fig. 1(b) was approximated by cylindrical segments of radii ranging from 0.3–4 cm; the resulting model

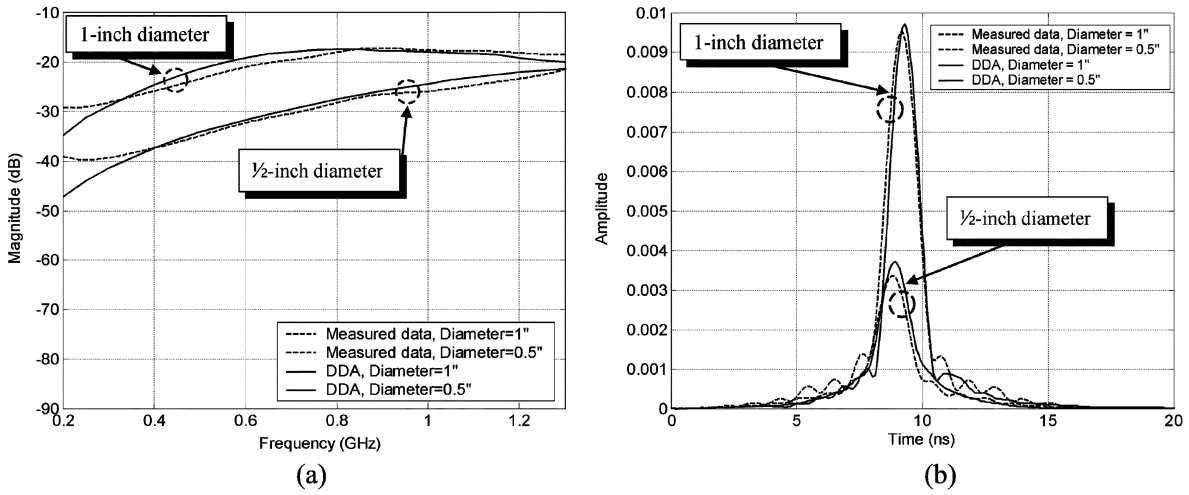

Fig. 7. Backscattered field intensity for two dielectric rods with different diameters buried in sand. (a) Frequency-domain response. (b) Time-domain response.

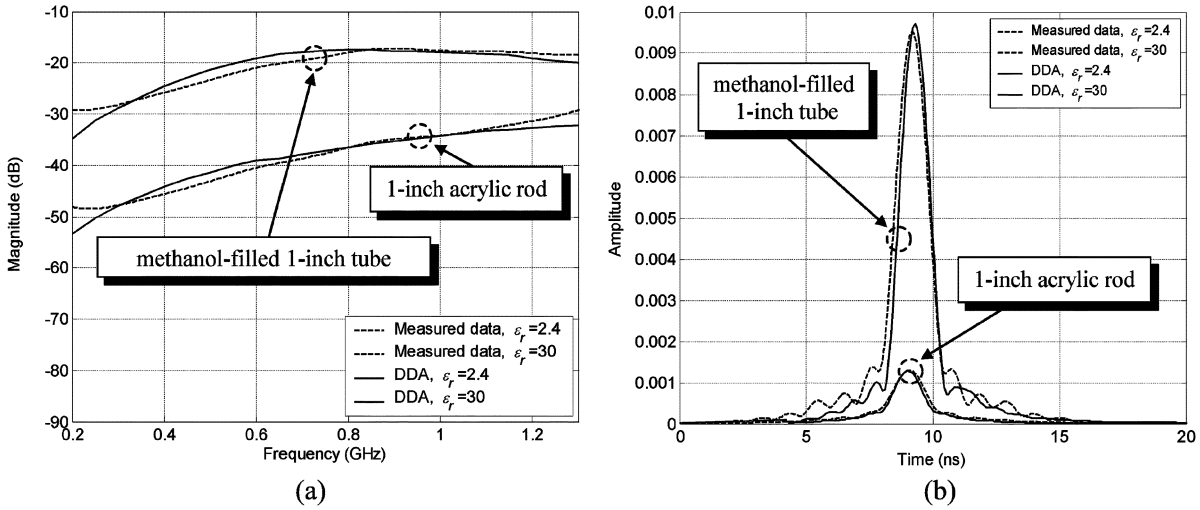

Fig. 8. Intensity of the backscattered fields for two 1-in rods with different permittivity values buried in sand. (a) Frequency-domain response. (b) Time-domain response.

is shown in Fig. 9. Based on measurements of the root water content and models in the literature, the root's complex dielectric constant was estimated to be approximately $20+10i$ over the frequency range of interest [32]. The large root mass that appears near the center of Fig. 1(b) was represented by a group of densely packed cylinders as shown in Fig. 9. To produce "random" realizations of GPR scattering by dense root structures, we selected several points in Fig. 9 where high root densities were present for simulation. The choice of positions located only over high root density locations was made to observe the maximum effects that could be generated by subsurface roots.

DDA calculations that take into account all root segments in Fig. 9 at every antenna position are computationally expensive, because of the large number of unknowns. Fortunately, physical considerations allow us to mitigate the problem. In general, soil is lossy, which limits the propagation distances of interest. In addition, the antenna has a mildly directional pattern, which

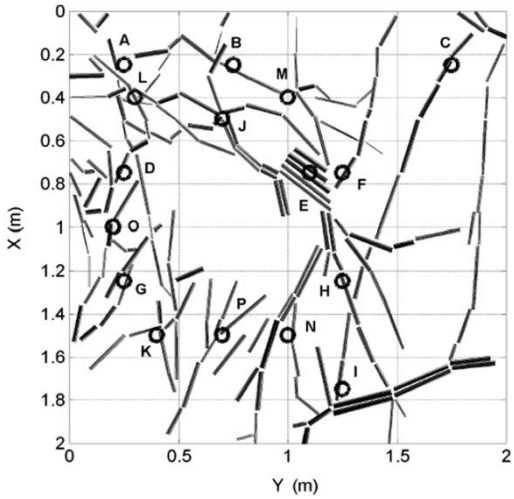

Fig. 9. Cylinder representation of root configuration from field measurements. The sample points selected as realizations of a high-density root environment are indicated by letters.

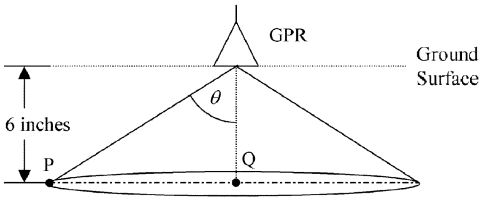

Fig. 10. Only roots in a circular cone shape are considered in the scattering computation.

limits its effective field of view. These facts imply that roots far from the antenna or outside the pattern will have little contribution to the scattered fields. Thus, instead of considering all roots at each antenna position, it is sufficient to consider only those roots that both lie within some distance from the source and are within the pattern of the antenna. Dielectric measurements of the soil from the field test site showed a dielectric constant of 5 and a conductivity of 0.0035 S/m. For a dipole source placed on such a medium, only the root segments within the cone shown in Fig. 10 need to be considered in the calculation. The angle θ is 76.8°, which is defined by the criterion that the incident field intensity at Point P is at least 25 dB below that at Point Q. To give a general idea how large the problem is, let us consider a case which the antenna is placed directly over the root mass. The total number of unknowns involved at 1 GHz is 9960, and the total time it takes to perform a frequency scan from 0.05–1.0 GHz with a 0.05-GHz step is 2.62 h on the same computer mentioned in Section III-B.

A limitation of the volumetric DDA code formulation involves its applicability for metallic targets, such as the standard "105-mm" shell often used in UXO studies. To avoid this problem, this shell was modeled as a dielectric object (40 cm in length and 10 cm in diameter) with relative permittivity $1 + 20i$. Because modeling the shell as a dielectric object reduces the target scattering obtained, comparing amplitudes of the response of this target to those of the roots alone is not of interest in this case. However, interaction effects between the roots and target are not strongly influenced by the use of a dielectric target model, particularly if the dominant root–target interaction is a shadowing or attenuation of the field incident upon the target due to the presence of roots. To examine root–target interaction effects, simulations were performed for roots both with and without the target present, and the results were subtracted to obtain contributions from the target in the presence of roots. When compared to target results computed in the absence of roots, only minor differences were observed. These differences showed only a very slight attenuation and time shift of the target return due to the presence of roots. Due to these results, the following analyses simply consider comparisons of returns from roots alone to those from a metallic target alone. Metallic target return amplitudes were obtained from the FDTD code described in [30].

A statistical model for GPR performance was developed as follows. We assume that the radar emits a (complex) waveform $h(t)$. We further assume that the target response is dominated by the specular return, which can be expressed as $Ah(t-\tau_1)$, in which τ_1 is a time delay and A is a complex scalar that accounts for both propagation losses and a possible change in phase due

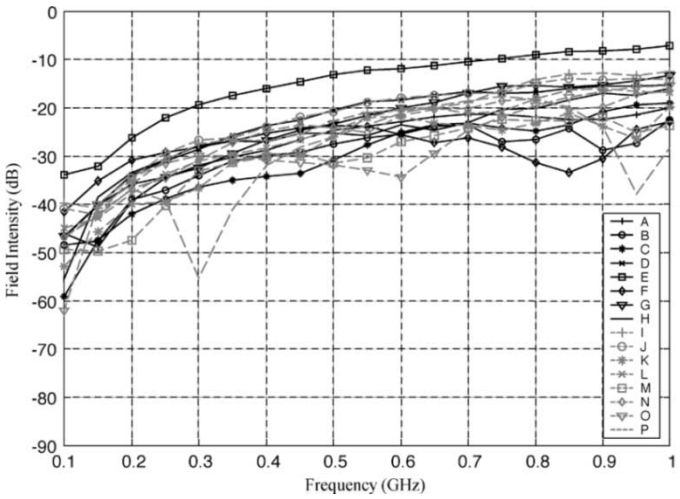

Fig. 11. Sixteen examples of clutter spectra computed over known root locations.

to reflection. The root return is also approximated by its specular contribution, which we write as $Bh(t-\tau_2)$ in which τ_2 and B are an appropriate delay and a complex scalar, respectively. The effects of receiver noise are assumed to be insignificant in comparison to the clutter. Neglecting root–target interaction effects, the detection problem can be expressed as follows:

$$x(t) = \begin{cases} Ah(t-\tau_1) + Bh(t-\tau_2), & \text{if} H_1 \\ Bh(t-\tau_2), & \text{if } H_0 \end{cases} \tag{8}$$

in which $x(t)$ is the measured signal, and H_0 (H_1) is the hypothesis that the target is absent (present) in the measurement. Matched-filter detection of this signal would produce the waveforms

$$x(t) \otimes h^*(-t) = \begin{cases} Av(t-\tau_1) + Bv(t-\tau_2), & \text{if } H_1 \\ Bv(t-\tau_2), & \text{if } H_0 \end{cases} \tag{9}$$

in which $v(t) = h(t) \otimes h^*(-t)$ is the response of the matched filter to the transmitted waveform. In practice, one could search the matched filter output for local maxima. A detection decision would be performed for each maximum.

When the targets and roots are consistently found at different depths, then range gating is an appropriate and effective approach to detection. The case of interest here, however, is when the target and roots cannot be separated by gating. As an estimate of worst case conditions, we take $\tau_1 \approx \tau_2$. If v_0 is the maximum value of $v(t)$, then the detection problem is equivalent to a test of the scalar

$$u \equiv \frac{\max\left[|x(t) \otimes h^*(-t)|\right]}{v_0} = \begin{cases} |A+B|, & \text{if } H_1 \\ |B|, & \text{if } H_0 \end{cases}. \tag{10}$$

The probability densities of $|A+B|$ and/or $|B|$ are required to make further progress. Consider first the density of $|B|$. Fig. 11 shows the clutter spectra for the 16 locations of high root density indicated in Fig. 9. The spectra indicate that the clutter is strongly non-Gaussian. On the logarithmic (decibel) scale used here, there is evidence of central tendency, and it is plausible to approximate the probability density values with a log-normal density $f(u)$ given by

$$f(u)du = \frac{1}{\sqrt{2\pi}\sigma u} e^{\frac{-(\ln(u)-\mu)^2}{(2\sigma^2)}} du \tag{11}$$

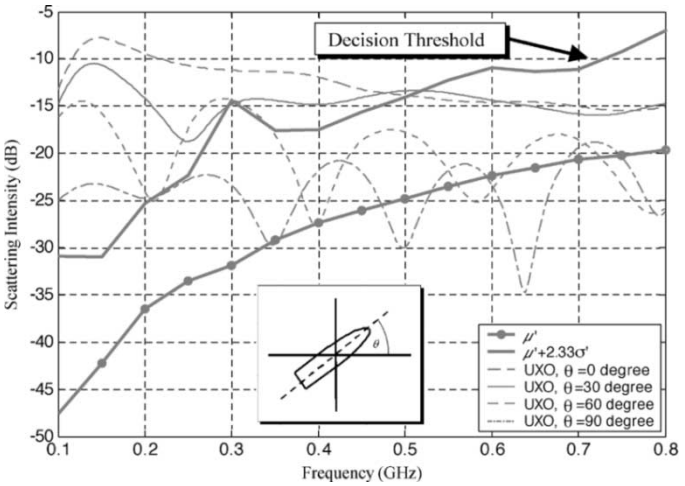

Fig. 12. Detectability calculations for a 105-mm shell in roots. The dark solid line at $\mu' + 2.33\sigma'$ is the decision threshold for a false-alarm rate of $0.01/\mathrm{m}^2$ (1-m^2 sensor pixels assumed).

where μ and σ are constants. If $s = 20\log_{10}(u) = 20v/\ln(10)$ is the value of the clutter return expressed in decibels, then

$$f(u)du = \frac{1}{\sqrt{2\pi}\sigma'} e^{\frac{-(s-\mu')^2}{(2\sigma'^2)}} ds \tag{12}$$

which is a standard normal density with the standard deviation $\sigma' = 20\sigma/\ln(10)$ and mean $\mu' = 20\mu/\ln(10)$ (both expressed in decibels). These quantities can be computed directly from the data expressed in decibels.

Confidence intervals for this density are readily obtained from those for a standard normal density, and they permit us to define appropriate detection thresholds to achieve a specific probability of false alarms. For $P_{fa} = 0.1$, the appropriate detection threshold in decibels is $\mu' + 1.28\sigma'$, and for $P_{fa} = 0.01$, the appropriate detection threshold is $\mu' + 2.33\sigma'$. The relevant false-alarm rate is obtained by dividing these probabilities by the sensor's pixel area.

The foregoing analysis is illustrated in Fig. 12, where we show the backscattered response of the 105-mm shell at depth 0.35 m computed via FDTD for several shell angles [30].[2] For orientation angle of less than 60°, this target displays a modest natural resonance at a frequency of 150 MHz. The target response is superimposed on the average clutter spectrum of Fig. 11 and on the (frequency-dependent) decision threshold for a false-alarm rate of $0.01/\mathrm{m}^2$ (assuming 1-m^2 sensor pixels). The figure suggests that for most UXO orientations and sensor frequencies, the target response exceeds the mean root clutter level, and hence, it will be detectable to some degree with a sensor having frequency content anywhere in the illustrated range. The figure also shows that detection at a false-alarm rate of $0.01/\mathrm{m}^2$ or better is only possible if the waveform has frequency content below 0.5 GHz. Based on these data, one expects better performance for low-frequency waveforms and significant challenges in achieving very low false-alarm rates. We also note that the scattered spectra for smaller UXO items would be shifted to higher frequency and would have a weaker RCS, i.e., poorer signal-to-clutter ratio.

[2]The UXO orientation in these results is nose-up, while real UXO will typically be found nose-down. For the purposes of this analysis, however, the difference in the target signature will be small.

V. Summary and Conclusion

We have examined the effect of buried biomass on GPR detection of UXO. A high biomass density site was excavated and analyzed to provide information for further modeling studies. A limit set of ground-contacting GPR data was acquired from this site, but unfortunately only over low biomass locations. The nature of the antenna of interest permits the scattered response to be calculated as if the antenna was immersed in an unbounded soil medium. That simplification was used throughout this paper.

A numerical solution based on the discrete dipole approximation (DDA) was developed to treat the complicated structures found in real roots. The code was validated by comparing it to a standard (MoM-based) BOR code and to GPR measurements of dielectric cylinders under controlled conditions. Good agreement was obtained.

Finally, a root structure excavated during the field measurements was studied in detail. These roots were discretized and represented by an ensemble of cylindrical segments having variable radii. The effect of roots on GPR detection performance was studied. Simulations including both root and (dielectric) target structures showed that the presence of roots altered target responses only slightly, so that simple comparisons of root only and target only returns are reasonable. Scattered responses at various points over the realistic root structure were computed and fitted to a log-normal probability density. Analysis showed that this root-related clutter would produce high false-alarm rates, particularly for sensors that had significant frequency content above about 0.5 GHz. The results suggest that the primary effect of roots is to add a randomly distributed set of discrete clutter sources and that any root-related loss in performance can be partially offset by using lower frequencies.

Acknowledgment

Technical direction was provided by K. Kappra and J. Sichna. Special thanks are due to C. Delucca for his support of the field work and to G. Smith for his careful measurements of soil properties. This work was sponsored by R. Harmon at the U.S. Army Research Office.

References

[1] *Proc. 9th Int. Conf. Ground Penetrating Radar*, Santa Barbara, CA, 2002.

[2] S. F. Mahmoud, S. M. Ali, and J. R. Wait, "Electromagnetic scattering from a buried cylindrical inhomogeneity inside a lossy earth," *Radio Sci.*, vol. 16, pp. 1285–1298, Nov.–Dec. 1981.

[3] G. Lombardi, G. Manara, G. Pelosi, and G. Toso, "Scattering by buried dielectric objects: Volumetric integral equation approach," in *Proc. IGARSS*, vol. 1, 1995, pp. 24–26.

[4] N. P. Zhuck and A. G. Yarovoy, "Two-dimensional scattering from an inhomogeneous dielectric cylinder embedded in a stratified medium: Case of TM polarization," *IEEE Trans. Antennas Propagat.*, vol. 42, pp. 16–21, Jan. 1994.

[5] C. M. Butler and X. B. Xu, "TE scattering by partially buried and coupled cylinders at the interface between two media," *IEEE Trans. Antennas Propagat.*, vol. 38, pp. 1829–1990, Nov. 1990.

[6] X. B. Xu and C. M. Butler, "Current induced by TE excitation on coupled and partially buried cylinders at the interface between two media," *IEEE Trans. Antennas Propagat.*, vol. 38, pp. 1823–1990, Nov. 1990.
[7] K. A. Michalski and D. Zheng, "Electromagnetic scattering and radiation by surfaces of arbitrary shape in layered media, part I: Theory," *IEEE Trans. Antennas Propagat.*, vol. 38, pp. 335–343, Mar. 1990.
[8] T. J. Cui and A. Herschlein, "Electromagnetic scattering by multiple three-dimensional scatterers buried under multilayered media, part I: Theory," *IEEE Trans. Geosci. Remote Sensing*, vol. 36, pp. 526–534, Mar. 1998.
[9] F. Baumgartner, J. Munk, J. Daniels, and C. C. Chen, "GPR scattering of dielectric cylinders," in *Proc. 7th Int. GPR Conf.*, 1998.
[10] J. Radzevicius, C. C. Chen, L. Peters, Jr., and J. Daniels, "Near-field dipole radiation dynamics through FDTD modeling," *J. Appl. Geophys.*, vol. 52, pp. 75–91, 2003.
[11] T. J. Cui and W. C. Chew, "Fast algorithm for electromagnetic scattering by buried 3-D dielectric objects of large size," *IEEE Trans. Geosci. Remote Sensing*, vol. 37, pp. 2597–2608, Sept. 1999.
[12] ——, "Fast evaluation of Sommerfeld integrals for EM scattering and radiation by three-dimensional buried objects," *IEEE Trans. Geosci. Remote Sensing*, vol. GE-37, pp. 887–900, Mar. 1999.
[13] A. Sullivan, "Model-based summary conclusions on the use of UWB radar for detecting unexploded ordnance," *Proc. SPIE.*, vol. 4742, pp. 291–302, Apr. 2002.
[14] M. Shenawee and C. M. Rappaport, "Monte Carlo simulations for clutter statistics in minefields: AP-mine-like-target buried near a dielectric object beneath 2-D random rough ground surfaces," *IEEE Trans. Geosci. Remote Sensing*, vol. 40, pp. 1416–1426, June 2002.
[15] B. T. Draine and P. Flatau, "The discrete-dipole approximation for scattering calculations," *J. Opt. Soc. Amer. A*, vol. 11, no. 4, pp. 1491–1499, 1994.
[16] L. Tsang, J. A. Kong, K. H. Ding, and C. O. Ao, *Scattering of Electromagnetic Waves-Numerical Simulations*. New York: Wiley, 2001.
[17] N. Niltawach, J. T. Johnson, C. C. Chen, and B. A. Baertlein, "GPR performance in the presence of buried biomass: Final report: Part 1, Experimental findings," ElectroScience Lab, The Ohio State Univ., Columbus, Rep. 741 809-2, Sept. 2002.
[18] N. Niltawach, J. T. Johnson, C. C. Chen, and B. A. Baertlein, "GPR performance in the presence of buried biomass: Final report: Part 2, Simulation and analysis," ElectroScience Lab, The Ohio State Univ., Columbus, Rep. 741 809-3, Sept. 2002.
[19] C. C. Chen, "Development of Custom Dielectric-Loaded Horn Antenn," ElectroScience Lab, The Ohio State Univ., Columbus, Tech. Rep. 741 582-1, Feb. 2002.
[20] L.Lord Rayleigh, "On the electromagnetic theory of light," *Phil. Mag.*, vol. 12, no. 81, 1881.
[21] ——, "The dispersal of light by a dielectric cylinder," *Phil. Mag.*, vol. 36, no. 365, 1918.
[22] C. A. Balanis, *Advanced Engineering Electromagnetics*. New York: Wiley, 1989.
[23] G. T. Ruck, D. E. Barrick, W. D. Stuart, and C. K. Krichbaum, *Radar Cross Section Handbook*. New York: Plenum, 1970, vol. 1.
[24] W. C. Au, "Computational electromagnetics in microwave remote sensing," Ph.D. dissertation, Mass. Inst. Technol., Cambridge, 1994.
[25] P. Flatau, "Improvements in the discrete-dipole approximation method of computing scattering and absorption," *Opt. Lett.*, vol. 22, no. 16, pp. 1205–1207, 1997.
[26] J. M. Putnam and L. N. Medgyesi-Mitschang, "Electromagnetic scattering from axially inhomogeneous bodies of revolution," *IEEE Trans. Antennas Propagat.*, vol. AP-32, pp. 797–806, Mar. 1984.
[27] M. G. Andreasen, "Scattering from bodies of revolution," *IEEE Trans. Antennas Propagat.*, vol. AP-13, pp. 303–310, Mar. 1965.
[28] J. R. Mautz and R. F. Harrington, "Radiation and scattering from bodies of revolution," *Appl. Sci. Res.*, vol. 20, pp. 405–435, 1969.
[29] E. H. Newman, "A user's manual for the electromagnetic surface patch code: ESP Version 5," ElectroScience Lab., The Ohio State Univ., Columbus, July 1999.
[30] K. R. Rao, K.-H. Lee, C.-C. Chen, and R. Lee, "Application of full-polarimetric ground penetrating radar for buried UXO classification," ElectroScience Lab., The Ohio State Univ., Columbus, Tech. Rep. 738 520-1, Feb. 2001.
[31] C. C. Chen, M. B. Higgins, K. O'Neill, and R. Detsch, "UWB fully-polarimetric GPR classification of subsurface unexploded ordnance," *IEEE Trans. Geosci. Remote Sensing*, vol. 39, pp. 1221–1230, June 2001.
[32] F. T. Ulaby and M. A. El-Rayes, "Microwave dielectric spectrum of vegetation: part II: Dual-dispersion model," *IEEE Trans. Geosci. Remote Sensing*, vol. GE-5, pp. 550–557, 1987.

Nakasit Niltawach received the B.E. degree from Chulalongkorn University, Bangkok, Thailand, and the M.S. degree from The Ohio State University (OSU), Columbus, both in electrical engineering.

From 2001 to 2003, he was a Graduate Research Associate with the ElectroScience Laboratory, OSU. His research interests are in the areas of ground penetrating radar and remote sensing.

Chi-Chih Chen (S'92–M'97) was born in Taiwan, R.O.C, in 1966. He received the B.S.E.E. degree from the National Taiwan University, Taipei, in 1988, and the M.S.E.E. and Ph.D. degrees from The Ohio State University (OSU), Columbus, in 1993 and 1997, respectively.

He joined the ElectroScience Laboratory, OSU as a Postdoctoral Researcher in 1997, was a Senior Research Associate from 1999 to 2003, and became a Research Scientist in 2004. His research interests include ground-penetrating radar, UWB antenna development, radar target detection and classification methods, automobile radar systems, and miniature antenna designs.

Dr. Chen is a member of Sigma Xi and Phi Kappa Phi.

Joel T. Johnson (S'91–M'96–SM'03) received the B.E.E. degree from the Georgia Institute of Technology, Atlanta, in 1991, and the S.M. and Ph.D. degrees from the Massachusetts Institute of Technology, Cambridge, in 1993 and 1996, respectively.

He is currently an Associate Professor in the Department of Electrical Engineering and ElectroScience Laboratory, The Ohio State University, Columbus. His research interests are in the areas of microwave remote sensing, propagation, and electromagnetic wave theory.

Dr. Johnson is a member of International Union of Radio Science (URSI) Commissions B and F, as well as a member of Tau Beta Pi, Eta Kappa Nu, and Phi Kappa Phi. He received the 1993 Best Paper Award from the IEEE Geoscience and Remote Sensing Society, was named an Office of Naval Research Young Investigator, National Science Foundation Career awardee, and PECASE Award recipient in 1997, and was recognized by the U.S. National Committee of URSI as a Booker Fellow in 2002.

Brian A. Baertlein (S'88–M'89) received the Ph.D. degree in electrical engineering from the University of Arizona, Tucson, in 1988.

From 1995 to 2003, he was Research Scientist and Adjunct Associate Professor of electrical engineering at the ElectroScience Laboratory, The Ohio State University (OSU), Columbus. In 2003, he joined Lockheed Martin Aeronautics Company, Palmdale, CA. Before joining OSU, he was a Senior Scientist with several small businesses doing work for the U.S. Department of Defense and Department of Energy. His recent research has addressed detection of land mines using a variety of sensors, multisensor data fusion, radar system analysis, and modeling of electromagnetic phenomena in magnetic resonance imaging. Prior work includes studies of electromagnetic scattering and propagation phenomena, antennas, electromagnetic compatibility, sensor systems of various types, sensor fusion, and signal processing.

Dr. Baertlein is a member of Eta Kappa Nu, Tau Beta Pi, ACES, SPIE, and SAE.